

**ES2019-3893**

## **PARAMETRIC ANALYSIS OF PARTICLE CSP SYSTEM PERFORMANCE AND COST TO INTRINSIC PARTICLE PROPERTIES AND OPERATING CONDITIONS**

**Kevin J. Albrecht**

Sandia National Laboratories  
Albuquerque, NM, USA

**Matthew L. Bauer**

U.S. Department of Energy  
Washington, DC, USA

**Clifford K. Ho**

Sandia National Laboratories  
Albuquerque, NM, USA

### **ABSTRACT**

The use of solid particles as a heat-transfer fluid and thermal storage media for concentrating solar power is a promising candidate for meeting levelized cost of electricity (LCOE) targets for next-generation CSP concepts. Meeting these cost targets for a given system concept will require optimization of the particle heat-transfer fluid with simultaneous consideration of all system components and operating conditions. This paper explores the trade-offs in system operating conditions and particle thermophysical properties on the levelized cost of electricity through parametric analysis. A steady-state modeling methodology for design point simulations dispatched against typical meteorological year (TMY) data is presented, which includes computationally efficient submodels of a falling particle receiver, moving packed-bed heat exchanger, storage bin, particle lift, and recompression supercritical CO<sub>2</sub> (sCO<sub>2</sub>) cycle. The components selected for the baseline system configuration presents the most near-term realization of a particle-based CSP system that has been developed to date. However, the methodology could be extended to consider alternative particle receiver and heat exchanger concepts. The detailed system-level model coupled to component cost models is capable of propagating component design and performance information directly into the plant performance and economics. The system-level model is used to investigate how the levelized cost of electricity varies with changes in particle absorptivity, hot storage bin temperature, heat exchanger approach temperature, and sCO<sub>2</sub> cycle operating parameters. Trade-offs in system capital cost and solar-to-electric efficiency due to changes in the size of the heliostat field, storage bins, primary heat exchanger, and receiver efficiency are observed. Optimal system operating

conditions are reported, which approach levelized costs of electricity of \$0.06 kW<sub>e</sub><sup>-1</sup>hr<sup>-1</sup>.

### **INTRODUCTION**

Particle heat transfer medium is being investigated to improve thermal efficiency of concentrating solar power (CSP) plants through enabling the use of high-efficiency supercritical CO<sub>2</sub> (sCO<sub>2</sub>) power cycles. The improvement in solar-to-electric efficiency is targeted to reduce the levelized cost of electricity (LCOE) to values required for large-scale adoption of the technology [1]. Work to date has focused on component level research, development, and demonstration. However, system-level studies are needed to optimize operating conditions and evaluate trade-offs in thermophysical properties due to the coupled component interaction and cost.

System-level modeling for estimating LCOE for CSP plants is typically accomplished through the System Advisor Model (SAM) [2], which has been developed and refined by NREL. SAM has capabilities for techno-economic modeling of molten salt towers, but particle system techno-economic modeling must currently occur through the generic model. The inputs for the generic model need to be derived from component submodels, which reflect the size, performance, and particle selection to determine parameters such as receiver efficiency and cost per kW<sub>t</sub>, storage cost per kW<sub>t</sub>-hr, and heat exchanger cost per kW<sub>t</sub>. An alternative to using subcomponent models to populate the capital cost input for the SAM generic model is to develop a dedicated particle CSP techno-economic tool where the component submodels are solved with fidelity that can propagate component design information directly into the plant performance and economics. Within the following sections, a system-level process flow model of a particle CSP plant for

baseload application is developed with cost estimates for the components as well as a thermodynamic analysis and cost model of a sCO<sub>2</sub> power cycle.

## PRIOR WORK

Particles have been identified as a desirable heat transfer Medium for next generation CSP systems due to their stability over a wide temperature range, ability to be directly heated with concentrated sunlight, non-corrosive nature, and the ability to be contained without a hermetically sealed system. Some of the challenges that have faced particle systems have been low temperature rise for a single-pass falling particle receiver, low heat-transfer coefficients when heated or cooled indirectly (i.e., primary heat exchanger), and particle loss/attrition/erosion [3]. The economic considerations of a particle-based CSP system facing these challenges has yet to be fully addressed [1].

The economics of particle thermal energy storage as well as the falling particle receiver have been previously discussed by Ho [4]. Cost estimates for the solar thermal receiver (not including the tower and lift) were estimated to be \$45 kW<sub>t</sub><sup>-1</sup>, based on scaling of a prototype construction and performance. Including the tower and particle lifting equipment, receiver costs were found to be \$125 kW<sub>t</sub><sup>-1</sup>, which is below the 2020 cost target of \$150 kW<sub>t</sub><sup>-1</sup> [5]. In addition, the cost of a particle thermal energy storage subsystem was found to be \$22 kW<sub>t</sub><sup>-1</sup>. However, this was for a 400 °C temperature rise, which would require integration with a combined cycle where highly recuperated sCO<sub>2</sub> cycles have a much lower temperature rise.

Recent work by Ho et al. [6] has discussed the cost of sCO<sub>2</sub> cycle components and system configurations in relation to a particle CSP heat source. Power cycle thermal efficiency was found to outweigh the reduction in storage costs due to the increased temperature difference between the hot and cold storage bin (primary heat exchanger temperature rise) when considering alternative cycle configurations.

System-level modeling studies for particle-driven sCO<sub>2</sub> [7] and steam Rankine cycles [8] have been conducted by Buck et al. Increasing hot storage temperature (while holding turbine inlet temperature constant) was found to substantially reduce LCOE through simultaneously decreasing the size and cost of the storage bins and primary heat exchanger, which outweighs the additional cost incurred by the decrease in receiver efficiency. LCOE below \$0.06 kW<sub>e</sub><sup>-1</sup>hr<sup>-1</sup> was demonstrated, but the financial assumptions were different from those used to establish the SunShot metrics [9], so a comparison to the present model is difficult to establish. In addition, the operational considerations for a heat exchanger using particles at temperatures far above the design temperature of the pressure vessel needs to be evaluated.

The work to date on the economics of particle based CSP systems has either been deficient due to not considering all system components and limitations or not calculating the levelized cost of electricity through running the model against TMY data. The following sections detail the thermal models and cost estimates of the various system components as well as a

sensitivity analysis to thermophysical properties and operating conditions of the particle system and sCO<sub>2</sub> power cycle.

## PARTICLE SYSTEM MODELING

The particle thermal energy storage subsystem consists of the solar thermal receiver, primary power cycle heat exchanger, lifts, and storage bins. A simplified process flow diagram of the particle CSP system is given in Figure 1, which assumes the storage bins, primary heat exchanger and power cycle are located at ground level. Alternative configurations include a vertically integrated system [10] that stacks the storage bins to reduce the lifting costs and energy parasitics. However, the 100 MW<sub>e</sub> system considered here will only evaluate ground-based storage bins due to the unknown breakpoint where the cost of supporting large storage bin volumes and particle masses outweighs the reduction in lifting costs.

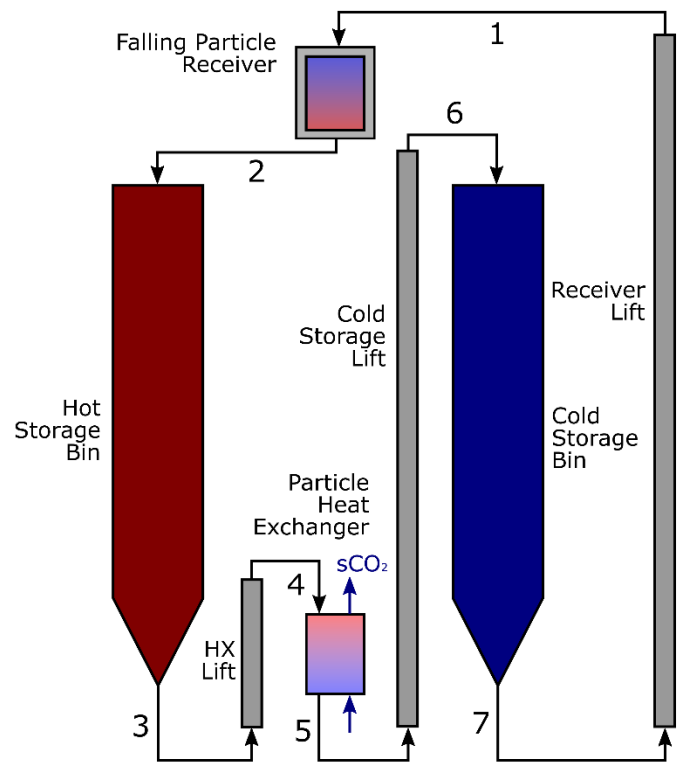


Figure 1. Particle thermal energy storage system configuration considering falling particle receiver with ground-level storage bins and sCO<sub>2</sub> power cycle for 100 MW<sub>e</sub> System

The particle system is modeled considering distributed models of the heat transfer components (receiver and heat exchanger) and lumped models of the storage bins and lift. All of the models are developed considering steady-state operation except for the level tracking in the storage bin. Provisions are included for calculating heat loss incurred in the particle lifting and storage components as well as the electrical energy consumption.

The receiver selected for this analysis is the falling particle receiver due to its mature state of development and demonstration [11, 12, 13, 14]. The receiver is modeled using a

reduced order model where the important physics are captured over a single dimension (y) in the fall direction. Previous researches have established the general technique for reduced order models of falling particle receivers [15, 16], which are implemented here. The 1-D conservation equations are given by the following equations where the velocity and curtain opacity have been compared to the experimental measurements of Ho et al. [17] and the thermal efficiency predictions have been compared to the CFD results of Mills and Ho [18].

$$0 = -\frac{d\phi_s t_c \rho_s v_s}{dy} \quad (1)$$

$$0 = -\frac{d\phi_s t_c \rho_s v_s^2}{dy} + \phi_s t_c \rho_s g \quad (2)$$

$$0 = -\frac{d\phi_s t_c \rho_s v_s h_s}{dy} + g_{c,front} - j_{c,front} + g_{c,back} - j_{c,back} - h_{conv} (T_s - T_o) \quad (3)$$

$$0 = \frac{d}{dy} \left( k_w \frac{dT_w}{dy} \right) + g_w - j_w - h_{conv} (T_w - T_o) \quad (4)$$

Particle-to-working fluid heat exchangers are being developed by several groups including Sandia [19, 20, 21], DLR [22], KSU [23], and CNRS-PROMES [24]. Three of the four system concepts have identified a moving packed-bed design as the preferred particle flow regime. The justification for the moving packed-bed design in the current system was discussed by Ho et al. [25]. The moving packed-bed heat exchanger performance implemented in this system was described by Albrecht et al. [19], which utilized coupled effectiveness number of transfer unit ( $\epsilon$ -NTU) calculations to determine overall heat transfer coefficients and required surface areas. The overall heat transfer coefficient is determined from Nusselt number correlations, which can be combined with thermophysical property data for sCO<sub>2</sub> and particle packed beds. In other words, the model is predictive of overall heat transfer coefficient based on heat exchanger geometry and particle properties. The shell-and-plate moving packed-bed heat exchanger is anticipated to achieve heat transfer coefficient approaching 450 W m<sup>-2</sup>K<sup>-1</sup> with plate spacing of 3 mm and particle diameters of 200  $\mu$ m.

The storage bin model calculates the required particle inventory ( $m_{s,st}$ ) and bin volume to achieve the specified storage ( $t_{st}$ ) based on the primary heat exchanger thermal input ( $\dot{Q}_{prime}$ ) and temperature difference between the hot and cold storage bins. The aspect ratio of the bins assumes a height to diameter ratio of two [7], which allows for the surface area to be determined for cost analysis. Future studies should evaluate the trade-off in construction cost and heat loss when changing the bin aspect ratio or considering several bins in parallel.

$$t_{st} \dot{Q}_{prime} = m_{s,st} (h_{s,4} - h_{s,5}) \quad (5)$$

The particle lifts are all assumed to be skip hoists, which are capable of reaching efficiencies ( $\eta_{lift}$ ) up to 80% with high-temperature particles [4]. High-temperature bucket elevators and Old's elevators have been utilized in small-scale systems [11], but higher lift efficiencies are desirable for a large commercial plant.

$$\dot{W}_{lift} = \frac{\dot{m}_s h_{lift} g}{\eta_{lift}} \quad (6)$$

The system of equations is solved inside of Engineering Equation Solver (EES) [26] where TMY data [27] is stored in a lookup table and a prescriptive dispatch strategy is defined to evaluate the useable solar resource through annual simulation. The energy accounting considers a minimum useable DNI for the falling particle receiver, maximum wind speed for heliostat deployment, and energy consumed during the start of the power cycle. Containing the model within EES allows for the use of subcomponent models with fidelity capable of capturing performance variations with changes in operating temperature, geometric parameters, and thermophysical properties. In addition, the thermophysical property database and heat transfer correlation library in EES allows for simplicity in particle/sCO<sub>2</sub> heat exchanger design studies and system boundary conditions derived from the sCO<sub>2</sub> cycle configuration and operating conditions. The baseline particle system design parameters are indicated in Table 1 for a baseload system with a net output of 100 MW<sub>e</sub>.

Table 1. Baseline system operating conditions and for a 100 MWe output

Parameter	Value	Units
TMY Data	Dagget, CA	
Net Output	100	MW <sub>e</sub>
Concentration Ratio	1200	
Receiver Height	200	m
Solar Multiple	2.5	
Storage	14	hr
Startup Time	0.5	hr
Hot Storage Temperature	800	°C
Approach Temperature	15	°C
Minimum DNI	500	W m <sup>-2</sup>
Maximum Wind Speed	15.65	mph
Optical Efficiency	50	%

## SUPERCRITICAL CO<sub>2</sub> POWER CYCLE

The ideal sCO<sub>2</sub> power cycle configuration for a dry-cooled CSP plant is the recompression closed Brayton cycle (RCBC) (Figure 2) [6, 28]. This cycle enables thermal efficiencies greater than 50% with dry cooling, which is mandated by the geographical constraints of CSP. To establish the solar-to-electric efficiency of the plant, it is important to first consider the power cycle operating conditions which establishes the thermal efficiency, primary heat exchanger temperature range (setting the minimum values for the hot and cold particle storage bins), and operating pressure and temperature for primary heat exchanger material selection. The cycle is modeled considering 0-D

thermodynamic models of the individual components with the performance metrics given in Table 2. The  $s\text{CO}_2/s\text{CO}_2$  recuperators are modeled with fixed approach temperatures where thermal duty plots are constructed from the boundary temperatures by discretizing the heat flow. This approach allows for the heat exchanger model to capture approach temperatures that occur at locations other than the inlet and outlet as well as a higher fidelity calculation of conductance.

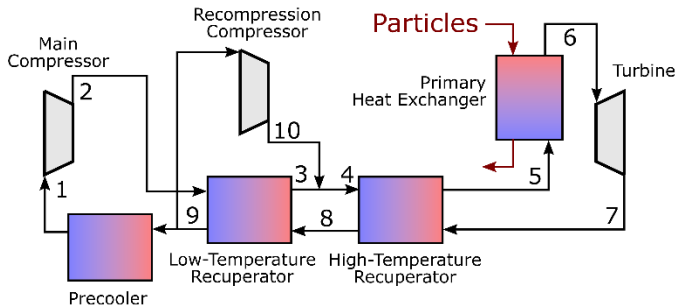


Figure 2. RCBC cycle configuration with a single heat addition and state points

Due to the complexity of the  $s\text{CO}_2$  cycle, it is important to consider how the performance of the cycle changes with operating parameters before combining with the particle CSP system. There are several variables affecting system performance including maximum pressure, turbine inlet temperature, compressor inlet temperature, pressure ratio, and recycle ratio.

The baseline system parameters for a solar driven  $s\text{CO}_2$  cycle are listed in Table 2. The optimized thermal efficiency for variations in the recycle ratio and pressure ratio leads to a thermal efficiency of 50.2% and a primary heat exchanger temperature rise of 149.7 °C. Since the cycle is highly-recuperated the temperature rise across the primary heat exchanger is very low. The low temperature rise results in difficulty storing thermal energy in a CSP system. Therefore, a parametric study of unoptimized pressure and recycle ratios could identify operating conditions with higher temperature rise for solar-driven  $s\text{CO}_2$  cycles valuing thermal energy storage. The system performance maps for variations in pressure ratio and recycle ratio are plotted in Figure 3. Optimal thermal efficiency is found at pressure and recycle ratios of 2.31 and 0.27, respectively. However, increases in primary heat exchanger temperature rise are possible with reductions in recycle ratio and increasing pressure ratio at the cost of thermal efficiency.

A typical approach to increasing power cycle thermal efficiency is to increase turbine inlet temperature or operating pressure. In order to understand these benefits on the  $s\text{CO}_2$  power cycle a parametric study is given in Figure 4, which identifies the baseline operating conditions and the potential benefits for increasing operating pressure and turbine inlet temperature. Increasing turbine inlet temperature and operating pressure are both shown to improve thermal efficiency and primary heat exchanger temperature rise. However, increases in either operating temperature or pressure could increase the cost of the primary heat exchanger. The operating pressure and temperature distribution in the primary heat exchanger determines the

fraction of surface area that needs to be constructed from expensive high-nickel alloys. Increasing turbine inlet temperature not only increases the primary heat exchanger  $s\text{CO}_2$  outlet temperature, but also the primary heat exchanger  $s\text{CO}_2$  inlet temperature, which shifts the entire device to a higher operating temperature.

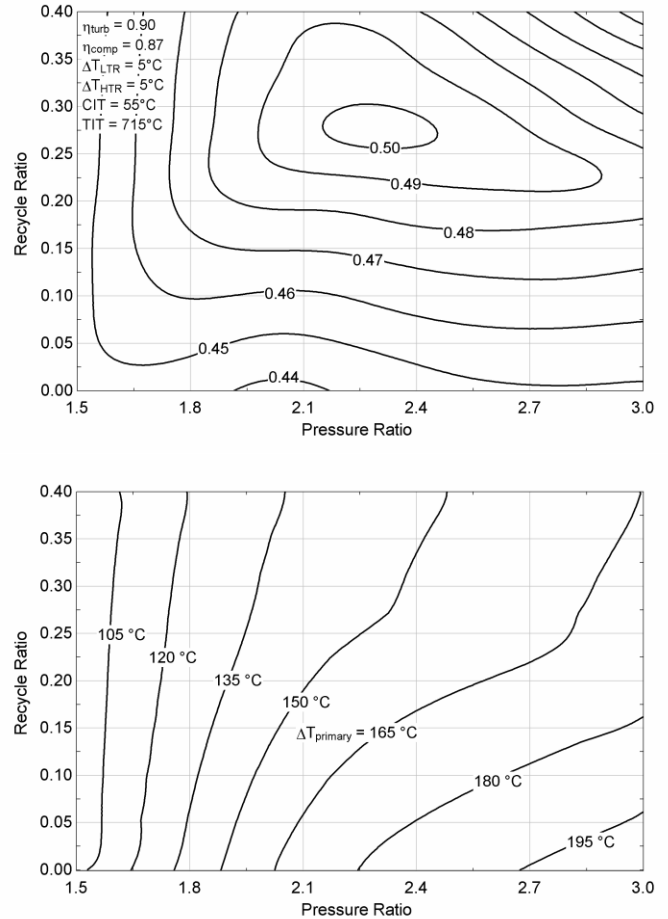


Figure 3. Thermal efficiency (top) and primary heat exchanger temperature rise (bottom) of the RCBC cycle as a function of pressure ratio and recycle ratio for fixed turbine (715 °C) and compressor (55 °C) inlet temperatures and maximum pressure (25 MPa)

To date, dry cooled  $s\text{CO}_2$  power cycles have been simulated by requiring a compressor inlet temperature of 55 °C, which assumes a maximum ambient temperature of 40 °C and a 15 °C approach temperature in the precooler [29]. However, significantly reduced compressor inlet temperatures are possible based on the time of day as well as day of year that the cycle is operated [30]. In addition, the possibility of reducing compressor inlet temperature through coupling with desalination technologies, heat pumping, or cold storage could provide decreases in compressor inlet when operating during times with elevated ambient temperature. A parametric study of compressor inlet temperature and maximum pressure is displayed in Figure 5. Reducing the compressor inlet temperature is shown to have a significant benefit on both the thermal efficiency and primary

heat exchanger temperature rise. If compressor inlet temperature of 35 °C can be obtained, the thermal efficiency will improve to 54% and the primary heat exchanger temperature rise can be increased by 40 °C to 190 °C. This improvement would result in a drastic reduction in the size of particle storage bins as well as decreased fraction of the primary heat exchanger that needs to be constructed from expensive high-nickel alloys. It is important to note that the temperature rise across the primary heat exchanger is increasing through lowering the sCO<sub>2</sub> inlet temperature, which shifts the heat exchanger to a lower operating temperature. However, such low compressor inlet temperatures might require the development of a compressor that can deal with liquid CO<sub>2</sub> [30].

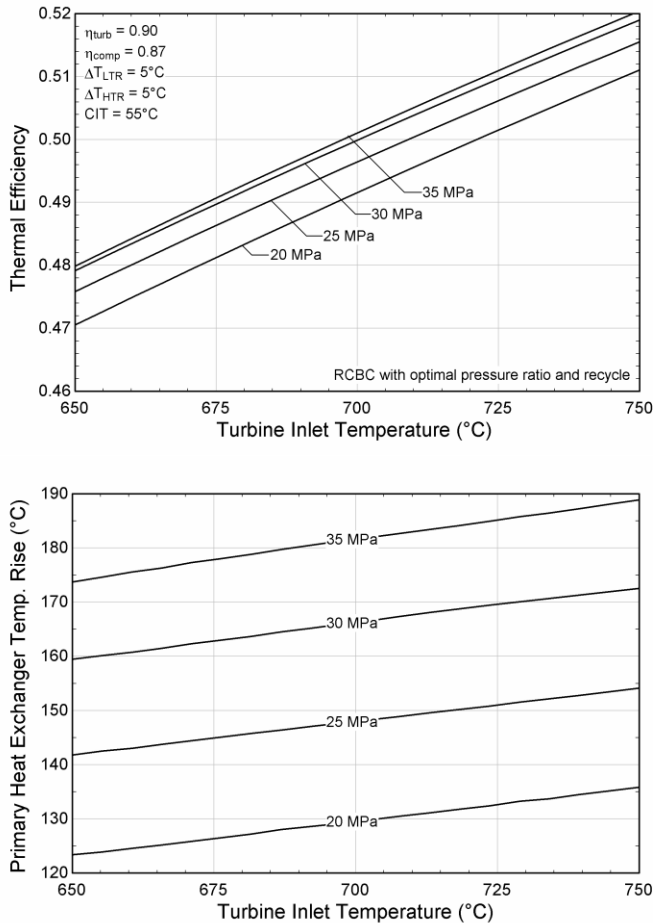


Figure 4. Sensitivity of the RCBC cycle thermal efficiency (top) and primary heat exchanger temperature rise (bottom) to turbine inlet temperature and maximum pressure with the recycle ratio and pressure ratio optimized for thermal efficiency

Beyond decreasing compressor inlet temperature, it is possible to reduce compressor parasitics and increase primary heat exchanger temperature rise through compressor intercooling. Furthermore, power cycle efficiency can be improved by performing several heat additions, which approximates isothermal expansion. This could prove to be advantageous because some of the high temperature heat addition of the primary heat exchanger would be shifted to an

intermediate sCO<sub>2</sub> pressure, which might alleviate some of the material strength requirements. However, this should be considered in future studies. The present analysis only considers a single heat addition step and no compressor intercooling for simplicity.

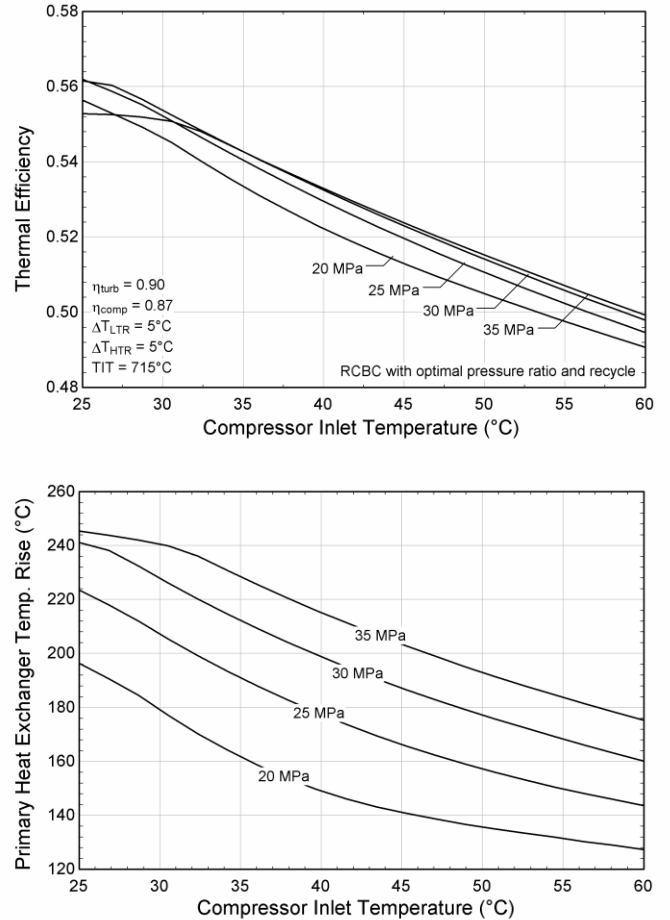


Figure 5. Sensitivity of the RCBC cycle thermal efficiency (top) and primary heat exchanger temperature rise (bottom) to compressor inlet temperature and maximum pressure with the recycle ratio and pressure ratio optimized for thermal efficiency

Table 2. Baseline component performance metrics for sCO<sub>2</sub> cycle modeling and particle system boundary conditions

Parameter	Value	Units
Turbine inlet temperature (TIT)	715	°C
Compressor inlet temperature (CIT)	55	°C
Operating pressure	25	MPa
LTR approach temperature	5	°C
HTR approach temperature	5	°C
Turbine isentropic efficiency	90	%
Compressor isentropic efficiency	87	%

## PARTICLE HEAT TRANSFER MEDIA

Thermophysical properties of the particle heat transfer media are important considerations in the design and optimization of particle-based CSP systems. Specific heat capacity, density, and solids volume fraction directly influence

the inventory and storage bin volume. In addition, properties that influence heat transfer such as particle size, thermal conductivity, emissivity, and solar absorptivity need to be considered, which affect the efficiency of the solar thermal receiver and heat transfer area of the primary heat exchanger.

Low cost naturally occurring material, such as red sand and olivine sand, are being considered, but the relatively low solar absorptivity and inhalation risks are a potential concern when used as a directly irradiated heat transfer material [31]. Higher cost engineered material, such as the sintered bauxite particles from CARBO Ceramics, have been shown to be durable, flowable, and stable at elevated temperature with high solar absorptivity [32]. The tradeoff in cost and thermophysical properties needs to be considered through a technoeconomic analysis of the entire system.

Bulk particle-to-particle heat transfer (effective thermal conductivity) of the particulate heat transfer material and the near-wall particle resistance are the dominate factors impacting heat transfer in the moving packed-bed heat exchanger [19]. Correlations are available to predict bulk effective thermal conductivity from intrinsic particle properties [33] (material conductivity, size, emissivity, and interstitial gas), which have been shown to be in good agreement with experimental data for the particles of interest [34].

Prior work has investigated the optimal particle size selection and geometry of the primary heat exchanger alone [19]. However, future work should look to optimize the particle size and perform sensitivity analysis to determine impacts of intrinsic particle properties on system performance. The parameters for the baseline particle selection of CARBO HSP 40/70 are given in Table 3.

Table 3. Thermophysical properties of CARBO HSP 40/70 sintered bauxite particles

Parameter	Value	Units
Solar weighted absorptance <sup>1</sup> [32]	0.92	-
Emissivity <sup>1</sup> [32]	0.85	-
Material thermal conductivity	2.0	W m <sup>-1</sup> K <sup>-1</sup>
Material density	3300	kg m <sup>-3</sup>
Packed volume fraction	0.60	-
Flowing volume fraction	0.55	-
Diameter	320	μm
Specific heat capacity [19]	148.2 T <sub>s</sub> <sup>0.3093</sup>	J kg K <sup>-1</sup>

<sup>1</sup>Reduced to capture intrinsic rather than packed bed values

## COMPONENT COST MODELS

The modeling techniques discussed in the previous sections can be used to size components and calculate solar-to-electric efficiencies and annual system production. However, the models must be combined with component cost models to inform plant design and operation based on the net economic benefit. The component cost models presented in this section have been derived from various literature sources to estimate the specific cost of the falling particle receiver, moving packed-bed shell-and-plate heat exchanger, and particle storage bins and heat transfer/energy storage material. The component cost metrics

have been constructed such that the cost metrics can be compared to the 2020 cost targets for the receiver, heat exchanger, thermal storage system, and power cycle.

The total cost of the receiver ( $C_{rec}$ ) is calculated as the cost of the falling particle receiver ( $C_{fpr}$ ), support tower ( $C_{tower}$ ), and receiver lift ( $C_{lift,rec}$ ).

$$C_{rec} = C_{fpr} + C_{tower} + C_{lift,rec} \quad (7)$$

The falling particle receiver cost is calculated as a function of aperture area ( $A_{ap}$ ) according to equation (8), which was back calculated from the cost estimated by Ho [4].

$$C_{fpr} = 37400 \left[ \frac{\$/m^2}{m^2} \right] A_{ap} \quad (8)$$

The tower cost is estimated according to equation (9), which was taken from the work of Buck [7].

$$C_{tower} = 157.44 \left[ \frac{\$/m^{1.9174}}{m^{1.9174}} \right] (h_{rec})^{1.9174} \quad (9)$$

The lift cost ( $C_{lift}$ ) are estimated according to equation (10), which was taken from the work of Repole and Jeter [35] assuming a linear scaling with lift height and mass flow rate.

$$C_{lift} = 58.37 \left[ \frac{\$/m \cdot kg}{m \cdot kg} \right] \cdot h_{lift} \dot{m}_s \quad (10)$$

The particle heat exchanger cost ( $C_{HX}$ ) is estimated according to equation (11), where the cost of the heat transfer surface area ( $c_{HX}$ ) is weighted by the particle side inlet temperature of the specific bank according to equation (12). The heat transfer surface area ( $A_{HX}$ ) weighting captures the need to use materials other than stainless steel at temperatures above 600 °C. The cost of the moving packed bed heat exchanger has been estimated to be \$1000 m<sup>-2</sup> of particle side heat transfer area based on PCHE cost data. The increase in cost at temperatures above 600 °C reflects the need to use more expensive nickel alloys. The cost is determined by the particle side temperature, which is required for safety consideration and actual heat exchanger geometry. Even though the temperature of the heat transfer surface closely follows the temperature of the sCO<sub>2</sub>, the strength requirement is set by the particle side temperature due to the possibility of thermally equilibrating with the particle temperature in the case of losing or reduced sCO<sub>2</sub> flow.

$$C_{HX} = \sum A_{HX,i} c_{HX,i} \quad (11)$$

$$c_{HX} = \begin{cases} 1000 \left[ \frac{\$/m^2}{m^2} \right] & T_{sin} < 600 \text{ °C} \\ 1000 \left[ \frac{\$/m^2}{m^2} \right] + 0.3 \left[ \frac{\$/m^2 \cdot \text{°C}^2}{m^2 \cdot \text{°C}^2} \right] (T_{sin} - 600 \text{ °C})^2 & T_{sin} \geq 600 \text{ °C} \end{cases} \quad (12)$$

The storage bin cost ( $C_{st}$ ) is calculated according to equation (13), which is the sum of the cost of the hot and cold storage bin [7] in addition to the cost of purchasing the particle inventory and the cost of making up any particles lost from the

system ( $C_{\text{makeup}}$ ). The cost of additional non-storage (NS) particles is included in the analysis, which are required for filling the heat exchanger. For the ground-based system considered here, both the lift for moving particles from the hot storage bin to the heat exchanger ( $C_{\text{lift,HX}}$ ) and the lift for moving particles from the heat exchanger outlet to the cold storage bin ( $C_{\text{lift,cold}}$ ) are considered to be part of the storage cost.

$$C_{\text{st}} = c_{\text{bin,hot}}SA_{\text{bin}} + c_{\text{bin,cold}}SA_{\text{bin}} + C_{\text{lift,HX}} + C_{\text{lift,cold}} + (1 + \text{NS})c_{\text{particle}}m_{\text{s,st}} + C_{\text{makeup}} \quad (13)$$

$$c_{\text{bin}} = 1230 \left[ \frac{\$/\text{m}^2}{\text{m}^2} \right] + 0.37 \left[ \frac{\$/\text{m}^2}{\text{m}^2} \right] \frac{T - 600}{400} \quad (14)$$

The cost of the particles lost from the system is calculated as a percentage of the particle mass passing through the receiver over a single year ( $m_{\text{rec,annual}}$ ) multiplied by the lifetime of the system in years ( $N_{\text{life}}$ ).

$$C_{\text{makeup}} = N_{\text{life}}c_{\text{particle}}m_{\text{rec,annual}}f_{\text{loss}} \quad (15)$$

The cost of the heliostat field ( $C_{\text{field}}$ ) is calculated from the required reflective area ( $A_{\text{field}}$ ) assuming an annual optical efficiency, concentration ratio, and the receiver design point thermal input based on the solar multiple. The heliostat field performance and costs are taken from SunShot 2020 targets [9] since the present effort is directed at modeling the thermal energy storage and transport system.

$$C_{\text{field}} = (c_{\text{heliostat}} + c_{\text{prep}})A_{\text{field}} \quad (16)$$

In addition to the particle CSP components, it is necessary to calculate the cost of the sCO<sub>2</sub> power cycle ( $C_{\text{cycle}}$ ) to determine the overall system capital cost and LCOE. The metrics used for the system components are indicated in Table 4, which are taken from the work of Ho et al. [6]. The total power cycle can be calculated according to (17) using the size and performance requirements derived from the thermodynamic cycle model.

$$C_{\text{cycle}} = (1 - f_{\text{red}}) \left[ C_{\text{comp,MC}} + C_{\text{comp,HC}} + C_{\text{recup,LTR}} + C_{\text{recup,HTR}} + C_{\text{turb}} \right] \quad (17)$$

The baseline RCBC configuration operating conditions indicated in Table 2 at the optimal recycle and pressure ratio result in a total power cycle cost estimate of \$1165 kW<sub>e</sub><sup>-1</sup> (not including the primary heat exchanger). This is far above the SunShot cost target of \$600 kW<sub>e</sub><sup>-1</sup>. However, the cost estimates are still based on small-scale components where cost reductions are anticipated with future development of 100 MW<sub>e</sub> equipment. For the present analysis, a cost reduction ( $f_{\text{red}}$ ) of 48.5% is assumed to bring the baseline power cycle cost in line with the

\$600 kW<sub>e</sub><sup>-1</sup> metric. However, the functional dependence of the system components on the operating conditions remains for capturing the effects of cycle operating conditions on capital cost.

Table 4. Summary of sCO<sub>2</sub> cycle component cost models taken from the work of Ho et al. [6]

Component	Cost Function
Compressor	$C_{\text{comp}} = 643.15 \left[ \frac{\$/\text{kW}^{0.9142}}{\text{kW}^{0.9142}} \right] (\dot{W}_{\text{comp}})^{0.9142}$
Recuperator	$C_{\text{recup}} = 5.2 \left[ \frac{\$/\text{K}^{0.8933}}{\text{W}^{0.8933}} \right] (UA_{\text{recup}})^{0.8933}$
Turbine	$C_{\text{turb}} = 9923.7 \left[ \frac{\$/\text{kW}^{0.5886}}{\text{kW}^{0.5886}} \right] (\dot{W}_{\text{turb}})^{0.5886}$
Cooler	$C_{\text{cooler}} = 76.25 \left[ \frac{\$/\text{K}^{0.8919}}{\text{W}^{0.8919}} \right] (UA_{\text{cooler}})^{0.8919}$

Table 5. Baseline system parameters for estimating the levelized cost of electricity for an integrated particle CSP/sCO<sub>2</sub> system

Parameter	Value	Units
Particle Cost	1.0	\$ kg <sup>-1</sup>
Non-Storage Inventory	5	%
Particle Loss	0.0001	%
Heliostat Cost	75	\$ m <sup>-2</sup>
Site Preparation	10	\$ m <sup>-2</sup>
Contingency	10	%
Indirect	13	%
Construction	6	%
Financing	7	%
Lifetime	30	years
Operating and Maintenance	40	\$ kW <sub>e</sub> <sup>-1</sup> year <sup>-1</sup>

The total capital cost of the integrated particle CSP/sCO<sub>2</sub> system can be calculated through summing the contributions of the individual components.

$$C_{\text{cap}} = C_{\text{rec}} + C_{\text{HX}} + C_{\text{storage}} + C_{\text{field}} + C_{\text{cycle}} \quad (18)$$

In addition to the total capital cost, a comparison of the previously established SunShot path metrics [5] can provide insight into the anticipated cost distribution for a particle CSP system relative to the cost targets originally established to meet \$0.06 kW<sub>e</sub><sup>-1</sup>hr<sup>-1</sup>. The following equations present the component cost per kW<sub>t</sub> or per kW<sub>t</sub>hr and Table 6 summarizes these cost targets.

$$c_{\text{rec}} = \frac{C_{\text{rec}}}{\dot{Q}_{\text{rec}}} \quad (19)$$

$$c_{\text{HX}} = \frac{C_{\text{HX}}}{\dot{Q}_{\text{primary}}} \quad (20)$$

$$c_{\text{st}} = \frac{C_{\text{st}}}{q_{\text{st}}} \quad (21)$$

From the total capital cost, the LCOE can be calculated according to equation (22) where the total installed cost ( $IC_{\text{total}}$ ) and capital recovery factor (CRF) are calculated according to equations (23) and (24), respectively. The capacity

factor can be determined from the annual simulation as the fraction of time the power cycle is operating.

$$\text{LCOE} = \frac{\text{IC}_{\text{total}} N_{\text{life}} \text{CRF} + \text{OM} \dot{W}_{\text{net}} N_{\text{life}}}{W_{\text{elec,annual}} N_{\text{life}}} \quad (22)$$

$$\text{IC}_{\text{total}} = (1 + f_{\text{const}})(1 + f_{\text{indirect}}) \left[ (1 + f_{\text{cont}}) C_{\text{cap}} \right] \quad (23)$$

$$\text{CRF} = \frac{f(1+f)^N}{(1+f)^N - 1} \quad (24)$$

## DISCUSSION

Achieving levelized costs of electricity of  $\$0.06 \text{ kW}_e^{-1} \text{ hr}^{-1}$  is the 2020 cost target established by the SunShot vision study [9]. Subsequent analysis has established cost targets for individual system components, which illustrates a path and cost targets for developers of specific components. A comparison of component target cost metrics to the component cost metrics calculated for the baseline system configuration in this study to achieve  $\$0.06 \text{ kW}_e^{-1} \text{ hr}^{-1}$  is provided in Table 6. The falling particle receiver is observed to be significantly below the receiver cost target, which allows for the cost of the storage and heat exchanger to be above the targets and still approach  $\$0.06 \text{ kW}_e^{-1} \text{ hr}^{-1}$ . The remaining sections perform parametric studies of operating conditions and thermophysical properties to minimize LCOE.

Table 6. Comparison of the target component cost metrics and the component cost metrics for the baseline system configuration

Metric	Target [5]	Baseline
Receiver Cost ( $\$ \text{ kW}_t^{-1}$ )	150	95.63
Storage Cost ( $\$ \text{ kW}_t^{-1} \text{ hr}^{-1}$ )	15	17.79
Heat Exchanger Cost ( $\$ \text{ kW}_t^{-1}$ )	150	175.00
Power Cycle Cost ( $\$ \text{ kW}_e^{-1}$ )	600	600.00
Receiver Efficiency	90%	85.7%
Power Cycle Efficiency	55%	50.2%
Capacity Factor	69%	71%
LCOE ( $\$ \text{ kW}_e^{-1} \text{ hr}^{-1}$ )	0.06	0.0592

Two of the key design variables in any CSP plant are the solar multiple and the number of hours of storage. Baseload CSP systems are typically thought to have solar multiples above two and storage of 10 hours or greater. A parametric study for the baseline system operating conditions as a function of solar multiple and hours of storage is displayed in Figure 6. LCOE approaching  $\$0.06 \text{ kW}_e^{-1} \text{ hr}^{-1}$  is observed at solar multiples of 2.5 with storage hours of 14 or greater. Minimizing LCOE with these general system design parameters is in line with the anticipated system configuration of other studies [5].

The specification of operating conditions in terms of hot and cold storage temperature is another important design consideration for minimizing LCOE. A parametric study of hot storage temperature and heat exchanger approach temperature, which is the temperature difference between the cold storage bin and the  $\text{sCO}_2$  inlet temperature of the primary heat exchanger, is presented in Figure 7. Increasing the hot storage temperature is

shown to decrease the LCOE due to reducing the required particle inventory as well as reducing the total heat exchanger surface area. Even though the cost of the heat transfer surface area increases with temperature, the cost of the heat exchanger per  $\text{kW}_t$  is observed to reduce. Temperatures above  $800^\circ \text{C}$  are not considered in this study due to the extreme reduction in strength of high-temperature alloys and potential safety considerations when operating in a regime where the loss of  $\text{sCO}_2$  flow would result in heat exchanger damage or failure.

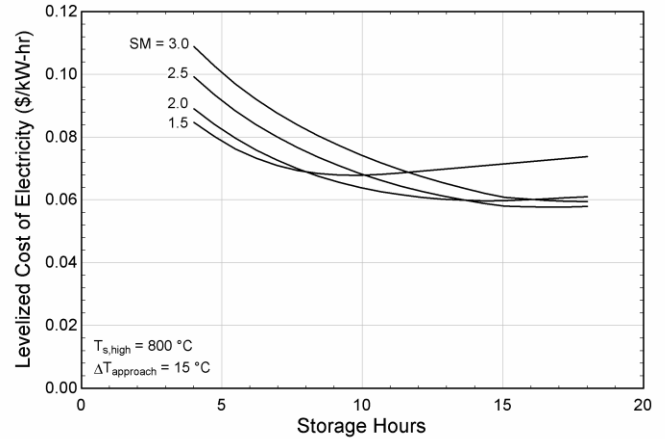


Figure 6. Particle CSP/ $\text{sCO}_2$  system levelized cost of electricity (LCOE) as a function of solar multiple (SM) and number of hours of storage

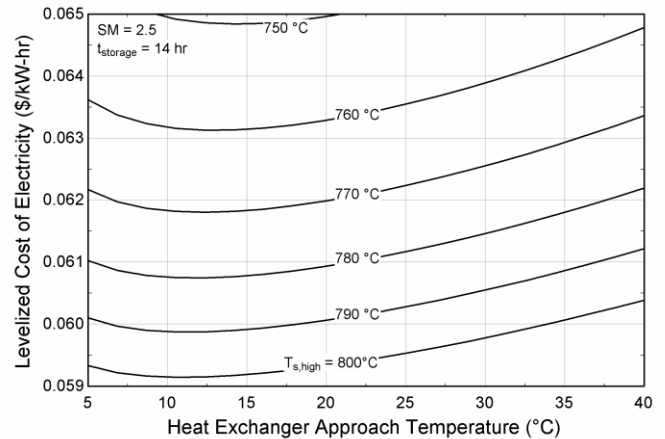


Figure 7. Particle CSP/ $\text{sCO}_2$  system levelized cost of electricity as a function of operating temperature for the hot storage bin and primary heat exchanger approach temperature

The approach temperature in the primary heat exchanger is the design parameter to optimize for setting the cold storage temperature. A low approach temperature is desirable for maximizing the temperature difference between the hot and cold storage to reduce the particle inventory and bin size. However, reducing the approach temperature requires large increases in heat transfer surface area due to the small heat transfer driving force. Figure 7 indicates minimum values of LCOE at heat exchanger approach temperatures of 12-15  $^\circ \text{C}$  depending on the hot storage temperature. It is important to note that this small

approach temperature occurs on the end of the heat exchanger constructed from lower cost materials.

The previous analysis considered operating the power cycle at conditions that maximize the thermal-to-electric conversion efficiency. However, as indicated in the RCBC parametric analysis, operating at conditions other than maximum thermal efficiency might result in lower LCOE when considering the coupled effects of the sCO<sub>2</sub> cycle and particle system. The LCOE of the integrated particle CSP/sCO<sub>2</sub> system is plotted in Figure 8 as a function of RCBC operating conditions. Comparing Figure 8 to Figure 3 illustrates the LCOE reduction that results from not operating the cycle at peak thermal efficiency. Increasing the pressure ratio and reducing the recycle ratio to increase the primary heat exchanger temperature rise is shown to reduce the overall LCOE. However, operating too far from the peak thermal efficiency results in reductions in LCOE as solar-to-electric efficiency continues to drop.

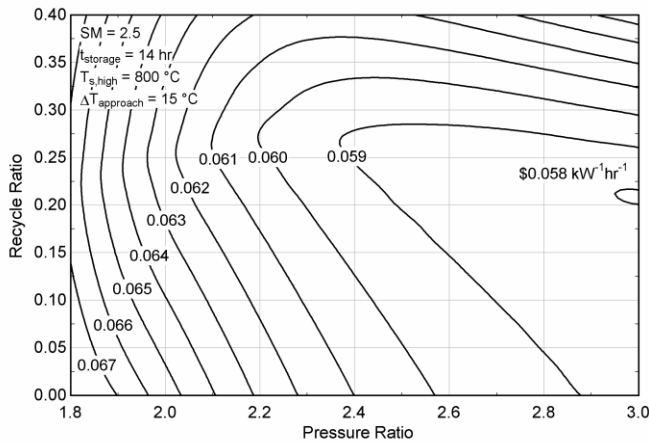


Figure 8. Levelized cost of electricity for the integrated particle CSP/sCO<sub>2</sub> system as a function of RCBC operating conditions

Alternative particles to sintered bauxite have been proposed including calcined flint clay, red sand and olivine sand [3, 31]. A system-level analysis considering the tradeoff between particle properties which influence the cost of storage, receiver performance, and heat exchanger performance is presented in Figure 9. It is important to note that the analysis does not consider additional safety concerns, erosion/abrasion, or particle handling considerations that can result from using non-engineered particles. The analysis is conducted by varying particle cost and absorptivity to determine the effect on LCOE, which can be used to identify combinations of absorptivity and cost that meet the \$0.06 kW<sub>e</sub><sup>-1</sup>hr<sup>-1</sup> target. The bound of zero cost particles establishes the minimum value of solar absorptivity for a specific LCOE target. For the present target of \$0.06 kW<sub>e</sub><sup>-1</sup>hr<sup>-1</sup>, particle solar absorptivity of 0.2 is required. In addition, the analysis illustrates the difficulty in achieving cost targets with particle costs above \$2 kg<sup>-1</sup> (even at absorptivity of 1.0).

The system model can also be used to establish targets for particle loss/attrition as a function of the particle cost. The analysis is displayed in Figure 10 where the loss is quantified as a fraction of the receiver flow rate and expressed on a log scale.

The system model allows for the additional cost incurred from particle replacement to be propagated into LCOE. The LCOE of a system with zero cost particles is not observed to be affected by particle loss. However, this analysis doesn't consider the thermal penalty of heating the makeup particles from ambient to the operating temperature. For particle cost of \$1 kg<sup>-1</sup>, the particle loss/attrition needs to remain below 0.001% to prevent significant impacts on LCOE.

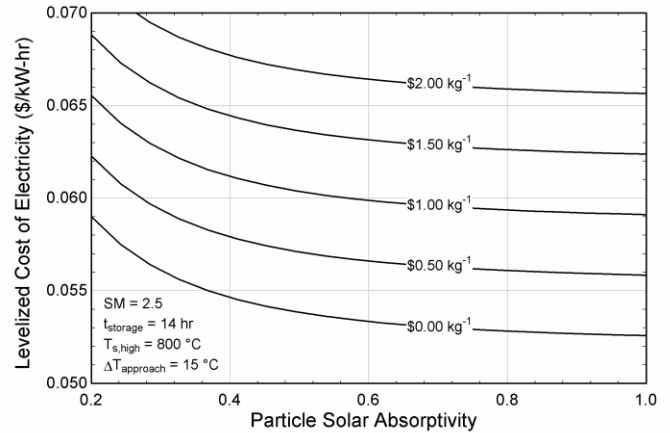


Figure 9. Particle CSP/sCO<sub>2</sub> system levelized cost of electricity as a function of particle cost and particle solar absorptivity for the baseline system operating parameters

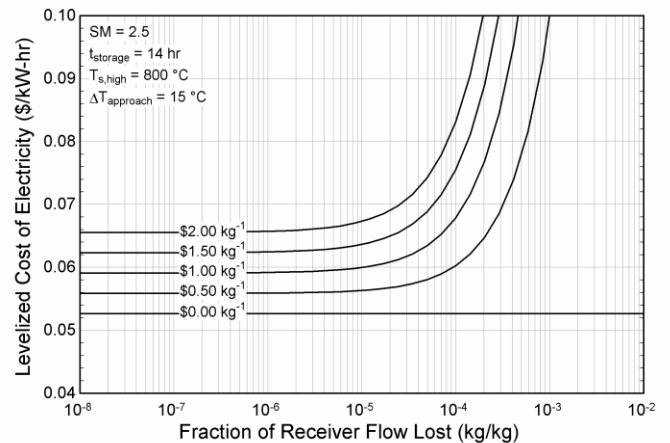


Figure 10. Particle CSP/sCO<sub>2</sub> system levelized cost of electricity as a function of particle cost and fraction of receiver flow lost to the ambient

## CONCLUSION

A fully coupled model of an integrated particle CSP system and RCBC sCO<sub>2</sub> cycle was constructed, which allows for simultaneous consideration of power cycle, solar collector, and thermal energy storage system operating conditions. The component submodels are of sufficient fidelity to propagate particle thermophysical properties and component geometric parameters into the plant economics. Optimal operating conditions and component sizes were identified through parametric studies of solar multiple, storage quantity, hot storage bin temperature, and primary heat exchanger approach

temperature. RCBC cycle operating parameters were also investigated when coupled to the particle CSP system. LCOE was found to be minimized at conditions not maximizing the thermal efficiency of the power cycle. Increasing pressure ratio to increase the primary heat exchanger temperature rise was found to reduce LCOE where the reduction in thermal energy storage costs outweighed the reduction in power cycle thermal efficiency. In addition, the tradeoff in particle cost and thermophysical properties was evaluated. The analysis showed that zero cost particles still require a minimum absorptivity to meet  $\$0.06 \text{ kW}_e^{-1}\text{hr}^{-1}$  and particle costs above  $\$2.0 \text{ kg}^{-1}$  are not likely to meet cost targets at any solar absorptivity.

## ACKNOWLEDGMENTS

Funding for this work is from DOE Solar Energy Technology Office (DE-FOA-0001697-1503). Sandia National Laboratories is a multimission laboratory managed and operated by National Technology and Engineering Solutions of Sandia, LLC., a wholly owned subsidiary of Honeywell International, Inc., for the U.S. Department of Energy's National Nuclear Security Administration under contract DE-NA0003525.

## NOMENCLATURE

$A$	Area ( $\text{m}^2$ )
$C_i$	Total cost of component $i$ (\$)
$c_i$	Specific cost of component $i$ ( $\$ \text{ unit}^{-1}$ )
CRF	Capital recovery factor
$f$	Fractional quantity
$g$	Gravitational constant ( $\text{m s}^{-2}$ )
$g_c$	Irradiance on curtain ( $\text{W m}^{-2}$ )
$h$	Enthalpy ( $\text{J kg}^{-1}$ )
IC	Installed cost (\$)
$j$	Radiosity ( $\text{W m}^{-2}$ )
$k$	Thermal conductivity ( $\text{W m}^{-1}\text{K}^{-1}$ )
$m$	Mass (kg)
$\dot{m}$	Mass flow rate ( $\text{kg s}^{-1}$ )
N	Number
NS	Non-storage fraction
OM	Operations and maintenance
$\dot{Q}$	Total heat flow (W)
$q$	Specific energy storage ( $\text{J kg}^{-1}$ )
$T$	Temperature ( $^{\circ}\text{C}$ )
$t$	Time (s)
$t_c$	Curtain thickness (m)
UA	Heat exchanger conductance ( $\text{W K}^{-1}$ )
$v$	Velocity ( $\text{m s}^{-1}$ )
$W$	Total work (J)
$\dot{W}$	Total power (W)

## Greek

$\rho$	Density ( $\text{kg m}^{-3}$ )
$\phi$	Volume fraction
$\eta$	Efficiency

## Subscript

annual	Annualized quantity
ap	Aperture
c	Curtain
comp	Compressor
const	Construction
cont	Contingency
conv	Convection
cooler	Heat rejection heat exchanger
cycle	Power cycle
elec	Electrical
field	Heliostat field
fpr	Falling particle receiver
HTR	High-temperature recuperator
HX	Heat exchanger
indirect	Indirect
life	Lifetime
lift	Lift
loss	Loss
LTR	Low-temperature recuperator
MC	Main compressor
o	Ambient condition
RC	Recompression compressor
rec	Receiver
recup	Recuperator
red	Reduction
s	Solid particles
st	Storage
turb	Turbine
w	Receiver back wall

## REFERENCES

- [1] M. Mehos, C. Turchi, J. Vidal, M. Wagner, Z. Ma, C. Ho, W. Kolb, C. Andraka and A. Kruiuzenga, "Concentrating Solar Power Gen3 Demonstration Roadmap," National Renewable Energy Laboratory, Golden, 2017.
- [2] "System Advisor Model Version 2017.9.5," National Renewable Energy Laboratory, Golden, 2017.
- [3] Z. Ma, G. Glatzmaier and M. Mehos, "Fluidized Bed Technology for Concentrating Solar Power With Thermal Energy Storage," *Journal of Solar Energy Engineering*, vol. 136, no. 3, p. 031014, 2014.
- [4] C. K. Ho, "A review of high-temperature particle receivers for concentrating solar power," *Applied Thermal Engineering*, vol. 109, pp. 958-969, 2016.
- [5] M. Mehos, C. Turchi, J. Jorgenson, P. Denholm, C. Ho and K. Armijo, "On the Path to SunShot: Advancing

- Concentrating Solar Power Technology, Performance, and Dispatchability," National Renewable Energy Laboratory, Golden, 2016.
- [6] C. K. Ho, M. Carlson, P. Garg and P. Kumar, "Technoeconomic Analysis of Alternative Solarized sCO<sub>2</sub> Brayton Cycle Configurations," *Journal of Solar Energy Engineering*, vol. 138, no. 5, pp. 051008-1-9, 2016.
- [7] R. Buck and S. Giuliano, "Impact of Solar Tower Design Parameters on sCO<sub>2</sub>-Based Solar Tower Plants," in *2nd European Supercritical CO<sub>2</sub> Conference*, Essen, 2018.
- [8] R. Buck and S. Giuliano, "CSP System Temperature Range Optimization for Reduced LCOE," in *SolarPACES2018*, Casablanca, 2018.
- [9] US DOE, "Sunshot vision study," Washington, DC, 2012.
- [10] C. K. Ho, "Gen 3 Particle Pilot Plant (G3P3): Integrated High-Temperature Particle System for CSP," in *Gen 3 CSP Kick-Off Meeting at the ASME 2018 Power and Energy Conference*, Lake Buena Vista, 2018.
- [11] C. Ho, J. Christian, D. Gill, A. Moya, S. Jeter, S. Abdel-Khalik, D. Sadowski, N. Siegel, H. Al-Ansary, L. Amsbeck, B. Gobereit and R. Buck, "Technology advancements for next generation falling particle receivers," *Energy Procedia*, vol. 49, pp. 398-407, 2014.
- [12] C. K. Ho, J. M. Christian, J. Yellowhair, K. Armijo, W. J. Kolb, S. Jeter, M. Golob and C. Nguyen, "Performance Evaluation of a High-Temperature Falling Particle Receiver," in *ASME 2016 10th International Conference on Energy Sustainability*, Charlotte, 2016.
- [13] C. K. Ho, J. M. Christian, J. Yellowhair, N. Siegel, S. Jeter, M. Golob, S. I. Abdel-Khalik, C. Nguyen and H. Al-Ansary, "On-sun testing of an advanced falling particle receiver system," in *AIP Conference Proceedings*, Cape Town, 2016.
- [14] N. P. Siegel, C. K. Ho, S. S. Khalsa and G. J. Kolb, "Development and Evaluation of a Prototype Solid Particle Receiver: On-Sun Testing and Model Validation," *Journal of Solar Energy Engineering*, vol. 132, no. 2, p. 021008, 2010.
- [15] M. Roger, L. Amsbeck, B. Gobereit and R. Buck, "Face-Down Solid Particle Receiver Using Recirculation," *Journal of Solar Energy Engineering*, vol. 133, no. 3, pp. 031009-1-8, 2011.
- [16] A. S. Oles and G. S. Jackson, "Modeling of a concentrated-solar, falling-particle receiver for ceria reduction," *Solar Energy*, vol. 122, pp. 126-147, 2015.
- [17] C. K. Ho, J. M. Chrisitan, D. Romano, J. Yellowhair, N. Siegel, L. Savoldi and R. Zanino, "Characterization of Particle Flow in a Free-Falling Solar Particle Receiver," *Journal of Solar Energy Engineering*, vol. 139, no. 2, pp. 021011-1-9, 2017.
- [18] B. Mills and C. K. Ho, "Annualized Thermal Performance of Intermediate-Scale Falling Particle Receivers," in *SolarPACES 2017*, Santiago, 2017.
- [19] K. J. Albrecht and C. K. Ho, "Design and operating considerations for a shell-and-plate, moving packed-bed, particle-to-sCO<sub>2</sub> heat exchanger," *Solar Energy*, vol. 178, pp. 331-340, 2019.
- [20] K. J. Albrecht and C. K. Ho, "Heat Transfer Models of Moving Packed-Bed Particle-to-sCO<sub>2</sub> Heat Exchangers," in *ASME 11th International Conference on Energy Sustainability*, Charlotte, 2017.
- [21] K. J. Albrecht and C. K. Ho, "High-Temperature Flow Testing and Heat Transfer for a Moving Packed-Bed Particle/sCO<sub>2</sub> Heat Exchanger".
- [22] T. Baumann and S. Zunft, "Development and performance assessment of a moving bed heat exchanger for solar central receiver power plants," *Energy Procedia*, vol. 69, no. 1, pp. 748-757, 2015.
- [23] A. El-Leathy, H. Al-Ansary, S. Jeter, E. Djajadiwinata, S. Alaql, M. Golob, C. Nguyen, R. Saad, T. Shafiq, S. Danish, S. Abdel-Khalik, Z. Al-Suhaibani, N. Abu-Shikhah, M. I. Haq, A. Al-Balawi and F. Al-Harhi, "Preliminary Tests of an Integrated Gas Turbine-Solar Particle Heating and Energy Storage System," in *AIP Conference Proceedings*, Santiago, 2018.
- [24] F. Gomez-Garcia, D. Gauthier and G. Flamant, "Design and performance of a multistages fluidised bed heat exchanger for particle-receiver solar power plants with storage," *Applied Energy*, vol. 190, pp. 510-523, 2017.
- [25] C. K. Ho, M. Carlson, K. J. Albrecht, Z. Ma, S. Jeter and C. M. Nguyen, "Evaluation of Alternative Designs fo a High Temperature Particle-to-sCO<sub>2</sub> Heat Exchanger," in *ASME 12th International Conference on Energy and Sustainability*, Lake Buena Vista, 2018.
- [26] S. Klein, *Engineering Equation Solver*, Natick: f-chart, 2016.
- [27] S. Wilcox and W. Marion, "Users Manual for TMY3 Data Sets," National Renewable Energy Laboratory, Golden, 2008.
- [28] W. H. Stein and R. Buck, "Advanced power cycles for concentrated solar power," *Solar Energy*, vol. 152, pp. 91-105, 2017.
- [29] C. S. Turchi, Z. Ma, T. W. Neises and M. J. Wagner, "Thermodynamic Study of Advanced Supercritical Carbon Dioxide Power Cycles for Concentrating Solar Power Systems," *Journal of Solar Energy Engineering*, vol. 135, no. 4, p. 041007, 2013.
- [30] R. Vijaykumar, M. Bauer, M. Lausten and A. Shultz, "Optimizing the Spercritical CO<sub>2</sub> Brayton Cycle for Concentrating Solar Power Application," in *The 6th International Spercritical CO<sub>2</sub> Power Cycles Symposium*, Pittsburgh, 2018.

- [31] H. Al-Ansary, A. El-Leathy, S. Jeter, E. Djajadiwinata, S. Alaqel, M. Golob, C. Nguyen, R. Saad, T. Shafiq, S. Danish, S. Abdel-Khalik, Z. Al-Suhaibani, N. Abu-Shikhah, M. I. Haq, A. Al-Balawi and F. Al-Harthi, "On-Sun Experiments on a Particle Heating Receiver with Red Sand as the Working Medium," in *AIP Conference Proceedings*, Santiago, 2018.
- [32] N. P. Siegel, M. D. Gross and R. Coury, "The Development of Direct Absorption and Storage Media for Falling Particle Solar Central Receivers," *Journal of Solar Energy Engineering*, vol. 137, 2015.
- [33] W. van Antwerpen, C. G. du Toit and P. G. Rousseau, "A review of correlations to model the packing structure and effective thermal conductivity in packed beds of mono-sized spherical particles," *Nuclear Engineering and Design*, vol. 240, no. 7, pp. 1803-1818, 2010.
- [34] T. Baumann and S. Zunft, "Properties of granular materials as heat transfer and storage medium in CSP application," *Solar Energy Materials & Solar Cells*, vol. 143, pp. 38-47, 2015.
- [35] K. D. Repole and S. M. Jeter, "Design and Analysis of a High Temperature Particulate Hoist for Proposed Particle Heating Concentrator Solar Power Systems," in *ASME 2016 10th International Conference on Energy Sustainability*, Charlotte, 2016.